zone, and this result rules out the possibility of the space group being $F\bar{4}3m$ rather than $Fd3m$.

We are indebted to Professor Mineo Kumazawa of Nagoya University and Professor Yoshito Matsui of Okayama University, who directed our attention to the present problem. We also thank Professor Kazuhiro Otsuka of Tsukuba University and Professor Nobuo Morimoto of Kyoto University for their interest in this problem.

References

HEUER, A. H. & MITCHELL, T. E. (1975). *J. Phys. C.* **8**, L541–L543.

HIRSH, P. B., HOWIE, A., NICHOLSON, R. B., PASHLEY, D. W. & WHELAN, M. J. (1965). *Electron Microscopy of Thin Crystals*, pp. 117–119. London: Butterworths.

HWANG, L., HEUER, A. H. & MITCHELL, T. E. (1973). *Philos. Mag.* **28**, 241–243.

MISHRA, R. K. & THOMAS, G. (1977). *Acta Cryst.* A**33**, 678.

NISHIKAWA, S. (1915). *Proc. Tokyo Math. Phys. Soc.* **8**, 199–209.

SAMUELSEN, E. J. & STEINSVOLL, O. (1975). *J. Phys. C*, **8**, L427–L429.

THOMPSON, P. & GRIMES, N. W. (1977). *J. Appl. Cryst.* **10**, 369–371.

Acta Cryst. (1980). A**36**, 126–134

Analysis of Multiple Inelastic Scattering of Electrons Incident on Crystalline Specimens

BY T. YAMAMOTO*

JEOL Ltd., Nakagami Akishima, Tokyo 196, *Japan*

(*Received* 21 *November* 1978; *accepted* 22 *August* 1979)

Abstract

An approximate expression is given for describing Bloch-wave amplitudes of electrons which undergo multiple inelastic scattering in crystalline specimens. The expression is derived from differential equations of inelastic scattering given by Howie [*Proc. R. Soc. London Ser. A* (1963), **271**, 268–287]. In the course of the derivation, the differential equations are reduced to a transport equation which has been applied to the analysis of multiple inelastic scattering in non-crystalline specimens. The identity between them is discussed, including the approximations employed. The expression was used to analyze Bloch-wave amplitudes of transmitted electrons at various thicknesses of copper and silicon crystals. It was found that the values of the amplitudes were sensitive to the shape of the interaction potential resulting from the excitation of core electrons. An accurate estimate of the potential will be required in future studies.

1. Introduction

The intensity of electrons passed through thin crystals shows a diffuse distribution around each diffraction spot and the distribution is normally anisotropic (*e.g.* Kikuchi patterns). This is due to the dynamical diffraction effect of inelastically scattered electrons. The theoretical study on the diffuse intensity was first made by Kainuma (1955) and subsequently by Takagi (1958*a*,*b*). Since then a number of theoretical studies have been made (Fujimoto & Kainuma, 1963; Okamoto, Ichinokawa & Ohtsuki, 1971). These theories succeeded in interpretating qualitative features of both Kikuchi lines and bands. It is well known, however, that the quantitative prediction is still unsatisfactory for thick specimens since the analysis is made within the framework of single inelastic scattering. Meanwhile, there is an increasing interest in analyzing diffraction patterns of bulk specimens which are obtained with reflective high-energy electrons and back-scattered electrons. In these cases, the effect of multiple inelastic scattering is so prominent that the knowledge as regards the behavior of diffusely scattered electrons is required in more detail.

Recently, several theoretical approaches to the analysis of multiple inelastic scattering have been proposed (Kamiya & Shimizu, 1976; Rez, 1978). In a previous report (Yamamoto, Mori & Ishida, 1978), the authors also attempted to deal with multiple inelastic scattering using a Monte Carlo method and studied the contrast of electron channelling patterns in scanning electron microscopy. In this approach, however, the

* Present address: Esco Ltd., Nishikubo 1-3-10, Musashino, Tokyo 180, Japan.

0567-7394/80/010126-09$01.00 © 1980 International Union of Crystallography

diffraction effect was excluded except for the first inelastic scattering. Generally, the main difficulty in theory is how to include the dynamical diffraction effect in multiple inelastic scattering. In the present paper, the multiple diffraction effect is treated more rigorously, and a simple expression of Bloch-wave amplitudes at various thicknesses is derived from differential equations of inelastic scattering given by Howie (1963). It is also shown that the present theory can readily be extended to the analysis of intensities of back-scattered electrons. The formula thus obtained is somewhat analogous to that derived for fluxes of inelastically scattered electrons in noncrystalline specimens based on a transport equation (Spencer, 1955; Dashen, 1964; Fathers & Rez, 1978). Physically, however, there is some difference between them: the quantities evaluated are stationary fluxes of electrons for the latter case whereas they are Bloch-wave amplitudes in the present theory.

The expression is further used to analyze intensities of electrons diffusely scattered around the incident direction in the case of relatively thin specimens. It is found that the calculated intensities are markedly affected by high- or medium-angle inelastic scattering *via* small-angle scattering which is caused by the excitation of core electrons. An accurate determination of the scattering cross section for this type of excitation will be desired in future studies because the main energy-loss process results from this excitation.

2. Theory

Basic processes of single inelastic scattering have been so far well understood in theory (Yoshioka, 1957; Takagi, 1958*a*,*b*; Whelan, 1965*a*,*b*). We first define several quantities which will be needed to describe scattering processes in the later formulation. To avoid confusion the theory is developed for transmitted electrons in thin specimens, and then extended for back-scattered electrons.

2.1. *Descriptions of inelastic scattering processes*

In a perfect crystal, the Bloch wave with wave vector $\mathbf{k}_n^i$ (i and n are the branch index and the energy level of the dispersion surface) induces the excitation of other Bloch waves due to inelastic scattering. Howie (1963) has shown that the relations among Bloch-wave amplitudes $\psi_m^j(z)$ of state $\mathbf{k}_m^j$ at a crystal depth of z are given by

$$\mathrm{d}\psi_m^j(z)/\mathrm{d}z = \sum_{\substack{n \\ n\neq m}} \sum_{i} c_{mn}^{ji} \exp(2\pi i \delta k_{mnz}^{ji})\, \psi_n^i(z), \quad (1)$$

where

$$c_{mn}^{ji} = -\left(\frac{mi}{2\pi\hbar^2 k_{mz}^j}\right) \sum_{g,h} C_g^j(\mathbf{k}_m^j)\, H_{g-h}^{mn}\, C_h^{i*}(\mathbf{k}_n^i) \quad (2)$$

and

$$\delta\mathbf{k}_{mn}^{ji} = \mathbf{k}_m^j + \mathbf{Q}_m - (\mathbf{k}_n^i + \mathbf{Q}_n), \quad (3)$$

in which case $C_g^i(\mathbf{k}_n^i)$ is the gth Fourier coefficient of the $\mathbf{k}_n^i$ Bloch wave, $\mathbf{Q}_m$ is the wave vector of the crystal excitation with state m and H_g^{mn} is the gth Fourier component of the interaction potential caused by the transition between crystal states m and n. In these equations, $\mathbf{k}_n^i$ and $\mathbf{Q}_m$ are restricted to the first Brillouin zone. In (2), k_{mz}^j means the z component of wave vector $\mathbf{k}_m^j$ (the z axis is parallel to the incident direction), and it can be approximated by k_m^j since we here confine ourselves to the intensity of electrons which are scattered slightly around the incident direction.

2.2. *The multislice method*

When the crystal is sliced into many thin layers, equation (1) can be integrated for each layer;

$$\psi_m^j(z+\Delta z) = \psi_m^j(z) + \sum_{\substack{n \\ n\neq m}} \sum_{i} c_{mn}^{ji} \exp(2\pi i \delta k_{mnz}^{ji} z) \times \{[\exp(2\pi i \delta k_{mnz}^{ji} \Delta z) - 1]/2\pi i \delta k_{mnz}^{ji}\}\, \psi_n^i(z),$$

where Δz is the thickness of the layer. If the thickness is small enough, the value within the curly brackets can be put equal to Δz, even for large values of δk_{mnz}^{ji}. Using the above relations, squared Bloch-wave amplitudes can be expressed as

$$\begin{aligned} |\psi_m^j(z+\Delta z)|^2 = {} & |\psi_m^j(z)|^2 + \Delta z \sum_{\substack{n \\ n\neq m}} \sum_{i} \{c_{mn}^{ji} \\ & \times \exp[2\pi i \delta k_{mnz}^{ji} z]\, \psi_n^i(z)\psi_m^{j*}(z) + c_{mn}^{ji*} \\ & \times \exp[-2\pi i \delta k_{mnz}^{ji} z]\, \psi_n^{i*}(z)\psi_m^j(z)\} \\ & + \Delta z^2 \sum_{i} \sum_{\substack{k \\ n\neq m \\ p\neq m}} \sum_{n,p} c_{mn}^{ji}\, c_{mp}^{jk*} \\ & \times \exp[2\pi i(\delta k_{mnz}^{ji} - \delta k_{mpz}^{jk})z] \\ & \times \psi_n^i(z)\psi_p^{k*}(z). \end{aligned} \quad (4)$$

Now we assume that $\psi_l^i(z)\psi_m^{j*}(z)$ can be neglected in (4) when either $l \neq m$ or $i \neq j$. The terms neglected give rise to interference parts in the intensity of diffusely scattered electrons, *i.e.* subsidiary fringes of Kikuchi lines. This fact has been shown in terms of the first-order perturbation theory (Fujimoto & Kainuma, 1963). These fringes are usually discerned with an appreciable intensity in diffraction patterns of thin crystals. The effect of the neglected terms will be discussed in a later section. On this assumption, we can obtain

$$|\psi_m^j(z+\Delta z)|^2 = |\psi_m^j(z)|^2 + \Delta z^2 \sum_{i} \sum_{\substack{n \\ n\neq m}} |c_{mn}^{ji}|^2\, |\psi_n^i(z)|^2. \quad (5)$$

This equation provides a simple picture for the analysis of inelastic scattering: the increase in the intensity of Bloch state (m,j), *i.e.* $|\psi_m^j(z+\Delta z)|^2 - |\psi_m^j(z)|^2$, is brought out by the transitions from all other Bloch states to the (m,j) state, as schematically shown by the solid lines in Fig. 1. On the other hand, there is a decrease in the intensity since the (m,j) state gives rise to the transitions from the state to all other states, as shown by the dotted lines.

When the transitions are collected by using equations similar to (4), the decrease is given by

$$\Delta z \sum_{\substack{n \\ n\neq m}} \sum_{i} |c_{nm}^{ij}|^2 \, |\psi_m^j(z)|^2.$$

As a result, the final expression of squared Bloch-wave amplitudes becomes

$$|\psi_m^j(z+\Delta z)|^2 = |\psi_m^j(z)|^2 + \Delta z^2 \sum_{\substack{i \\ n\neq m}} \sum_{n} |c_{mn}^{ji}|^2 \, |\psi_n^i(z)|^2 - \Delta z^2 \sum_{\substack{i \\ n\neq m}} \sum_{n} |c_{nm}^{ij}|^2 \, |\psi_m^j(z)|^2. \quad (6)$$

Now, we define matrix elements of single inelastic scattering for the transition from the (n,i) state to the (m,j) state

$$T_{mj,ni} = \begin{cases} \Delta z |c_{mn}^{ji}|^2, & \text{for } (m,j) \neq (n,i), \\ -\Delta z \sum_{j}' \sum_{m}' |c_{mn}^{ji}|^2, & \text{for } (m,j) = (n,i). \end{cases} \quad (7)$$

As will be later shown, $T_{mj,ni}$ is independent of layer thickness Δz which explicitly appears in (7). We also define the vector $\boldsymbol{\Phi}(z)$ which consists of the array of $|\psi_m^j(z)|^2$;

$$\boldsymbol{\Phi}(z) = \{\ldots, |\psi_m^j(z)|^2, \ldots\}.$$

Equation (6) can then be summarized in the matrix formula as follows:

$$\boldsymbol{\Phi}(z+\Delta z) = (\mathbf{E} + \Delta z \mathbf{T})\boldsymbol{\Phi}(z), \quad (8)$$

where $\mathbf{E}$ is the unit matrix. The squared Bloch-wave amplitudes are hereafter termed the excitation weights of the Bloch waves.

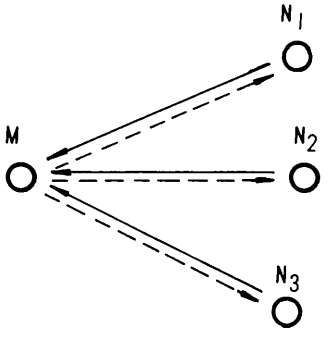

Fig. 1. Symbolic diagram of scattering processes.

2.3. *The elements of the transition matrix*

As seen in the derivation of (6), the diagonal element $T_{ni,ni}$ must coincide with the so-called absorption coefficient $\mu_i(\mathbf{k}_n^i)$ of the (n,i) Bloch state with opposite sign. To see this in another form, we substitute (2) into (7). In the present case, energy loss is much smaller than the energy of the incident electrons so that the difference between dispersion surfaces of the incident and inelastically scattered electrons can be neglected. Then we are able to omit suffixes m and j in $\mathbf{k}_m^j$, thereby specifying wave vectors $\mathbf{k}_n^i$ and $\mathbf{k}_m^j$ at the initial and scattered states as $\mathbf{k}$ and $\mathbf{k}'$, respectively. Absorption coefficient $-T_{\mathbf{k}i,\mathbf{k}i}$ in (7) becomes

$$\mu_i(\mathbf{k}) = \Delta z (m/2\pi\hbar^2 k)^2 \times \sum_{\mathbf{k}'} \sum_{h,h'} \sum_{g} \sum_{s} C_h^i(\mathbf{k}) C_{h'}^i(\mathbf{k}) H_{g-h}^s H_{g-h'}^{s*}, \quad (9)$$

where the summation over s is performed for all possible crystal excitation states.

It is shown in the phenomenological treatment that

$$\mu_i(\mathbf{k}) = (m/\pi\hbar^2 k) \sum_{h,h'} C_h^i(\mathbf{k}) \, V_{h-h'}' \, C_{h'}^i(\mathbf{k}), \quad (10)$$

where V_g' is the imaginary part of the gth Fourier component of the crystal potential. Comparing (9) with (10), we have

$$V_g' = \Delta z (m/4\pi\hbar^2 k) \sum_{\mathbf{k}'} \sum_{h} \sum_{s} H_{h-g}^s H_h^{s*}. \quad (11)$$

This is the same as the general expression of V_g' given by Whelan (1965*a*,*b*).

For simplicity, the specimen is assumed to be a mono-atomic crystal of simple cubic structure with centrosymmetry, and the wave-vector transfer of $\mathbf{k}' - \mathbf{k}$ is denoted by $\mathbf{q}_0$. It is shown that

$$H_g^s(\mathbf{q}_0) = H_g^{s*}(-\mathbf{q}_0) = \varphi(\mathbf{q}_0 + g) = \varphi(\mathbf{q}_g^-), \quad (12)$$

where φ is the function specified by the crystal excitation.

The summation over $\mathbf{k}'$ in (9) can be replaced in practice by the surface integral on the Ewald sphere

$$\Delta z \sum_{\mathbf{k}'} |c_{mn}^{ji}|^2 = v_1 k^2 \int |c_{mn}^{ji}|^2 \, \mathrm{d}\omega_q, \quad (13)$$

where v_1 is the volume of the thin layer and $\mathrm{d}\omega_q$ is the solid angle in the direction of $\mathbf{k}'$. It is convenient to introduce the quantity $S_{gh}(\mathbf{q}_0)$ which was used in the previous study (Yamamoto, Mori & Ishida 1978). Equation (9) can be written as

$$\mu_i(\mathbf{k}) = \int \sum_{g,h} S_{gh}(\mathbf{q}_0) \, C_g^i(\mathbf{k}) C_h^i(\mathbf{k}) \, \mathrm{d}\omega_q. \quad (14)$$

Comparing (9) with (13) and also by noting (12), we can obtain

$$S_{gh}(\mathbf{q}_0) = (m/2\pi\hbar^2)^2 v_1 \sum_s H_h^s(\mathbf{q}_0) H_g^{s*}(\mathbf{q}_0). \quad (15)$$

This quantity is independent of the crystal volume because H_g^s is normalized in the layer. As a result, (7) becomes

$$T_{k'j,ki} = \begin{cases} \Delta\omega_q \sum_{g,g'} \sum_{h,h'} C_g^j(\mathbf{k}') C_{g'}^j(\mathbf{k}') \\ \quad \times S_{g-h,g'-h'}(\mathbf{q}_0) C_h^i(\mathbf{k}) C_{h'}^i(\mathbf{k}), \\ \qquad\qquad \text{for } (\mathbf{k}',j) \neq (\mathbf{k},i), \\ -\mu_i(\mathbf{k}), \qquad \text{for } (\mathbf{k}',j) = (\mathbf{k},i), \end{cases} \quad (16)$$

where $\Delta\omega_q$ is the solid angle which the $(\mathbf{k}',j)$ state occupies around the $\mathbf{k}'$ direction on the Ewald sphere.

2.4. *Multiple inelastic scattering*

When the crystal is sliced into N layers with equi-thickness, $\boldsymbol{\Phi}(D)$ at the bottom ($z = D$) can be connected to $\boldsymbol{\Phi}(0)$ at the top surface using (8);

$$\boldsymbol{\Phi}(D) = (\mathbf{E} + D\mathbf{T}/N)^N \boldsymbol{\Phi}(0).$$

As N is increased, this tends to

$$\boldsymbol{\Phi}(D) = \exp(\mathbf{T}D)\, \boldsymbol{\Phi}(0), \quad (17)$$

where

$$\exp(\mathbf{T}z) = \mathbf{E} + z\mathbf{T} + z^2\,\mathbf{T}^2/2 + \ldots.$$

It can be shown from (7) that

$$\sum_{\mathbf{k}',j} T_{\mathbf{k}'j,ki} = \sum_{\mathbf{k},i} T_{\mathbf{k}'j,ki} = 0. \quad (18)$$

This equation, in conjunction with (17) and (18), provides

$$\sum_{\mathbf{k}',j} |\psi_{\mathbf{k}'}^j(z)|^2 = \sum_{\mathbf{k}',j} |\psi_{\mathbf{k}'}^j(0)|^2 = 1.$$

This relation implies the conservation of the total electron number at each crystal depth.

Moreover, if we find the orthogonal matrix $\mathbf{C}$ which enables $\mathbf{T}$ to be diagonalized,

$$\mathbf{TC} = \mathbf{C}\Lambda, \quad (19)$$

where Λ is the diagonal matrix consisting of eigenvalues for the transition matrix $\mathbf{T}$. By utilizing (19), (17) can be expressed as

$$\boldsymbol{\Phi}(z) = \mathbf{C} \exp(\Lambda z)\, \mathbf{C}^{-1}\, \boldsymbol{\Phi}(0). \quad (20)$$

2.5. *High-angle scattering*

The neglect of energy loss as well as the approximation of small-angle scattering in the preceding subsections cannot be used for treating intensities of electrons scattered at higher angles. We separate the excitation weights into $|\psi_F^j(z,\mathbf{k},m)|^2$ and $|\psi_B^j(z,\mathbf{k},m)|^2$, where m indicates the energy level and suffixes F and B mean Bloch waves proceeding in the forward and backward directions relative to the incident beam (for simplicity, we restrict ourselves to the analysis of inelastically scattered electrons at normal incidence). In addition, all excitation weights belonging to energy level m are represented by $\boldsymbol{\Phi}_F(z,m)$ and $\boldsymbol{\Phi}_B(z,m)$.

The excitation of phonons induces very small energy losses which allow us to neglect them practically. However, this excitation is responsible for high-angle scattering. In view of this, we separate the matrix elements of this excitation into $T_E^F(\mathbf{k}',j,n;\ \mathbf{k},i,n)$ and $T_E^B(\mathbf{k}',j,n;\ \mathbf{k},i,n)$ in the same manner as that applied to $\boldsymbol{\Phi}$.

Meanwhile, the excitation of core electrons and plasmons causes energy loss, inducing very small-angle scattering. The matrix of this excitation is denoted by $T_I(\mathbf{k}',j,m;\ \mathbf{k},i,n)$ for the transition from energy level n to m, in which case back-scattering is neglected.

It is somewhat lengthy to write down each element of the transition matrices $\mathbf{T}_I$, $\mathbf{T}_E^F$ and $\mathbf{T}_E^B$, so we only give some rules to modify (16) for the present case, taking into account the above definitions and noticing that:

(i) for $\mathbf{T}_I$, S_{gh} should be replaced by $S_{gh}^{\mathrm{cr}} + S_{gh}^{\mathrm{pl}}$ which result from the excitation of core electrons and plasmons, respectively;

(ii) for $\mathbf{T}_E^B$ and off-diagonal elements of $\mathbf{T}_E^F$, S_{gh} should be replaced by S_{gh}^{ph} resulting from the phonon excitation;

(iii) for diagonal elements of $\mathbf{T}_E^F$,

$$T_E^F(\mathbf{k},i,n;\ \mathbf{k},i,n) = -\sum_m \sum_{\mathbf{k}',j} T_I(\mathbf{k}',j,m;\ \mathbf{k},i,n) - \sum_{\mathbf{k}',j} [T_E^F(\mathbf{k}',j,n;\ \mathbf{k},i,n) + T_E^B(\mathbf{k}',j,n;\ \mathbf{k},i,n)]; \quad (21)$$

(iv) each element should be divided by $\cos\theta_m$ which is omitted in the approximation of small-angle scattering, where θ_m is the angle at which the electron is scattered with respect to the incident direction. In addition, $C^j(\mathbf{k}') \to C^j(\mathbf{k}_m)$ and $C^i(\mathbf{k}) \to C^i(\mathbf{k}_n)$.

The equation of connecting excitation weights at depth z to those at depth $z + \Delta z$ can be expressed as

$$\boldsymbol{\Phi}_F(z' + \Delta z', m) = [\mathbf{E} + \Delta z'\, \mathbf{T}_E^F(m,m)]\boldsymbol{\Phi}_F(z',m) + \Delta z'\, \mathbf{T}_E^B(m,m)\boldsymbol{\Phi}_B(z',m) + \Delta z' \sum_{n \leq m} \mathbf{T}_I(m,n)\boldsymbol{\Phi}_F(z',n), \quad (22a)$$

$$\boldsymbol{\Phi}_B(z'+\Delta z',m) = [\mathbf{E} - \Delta z'\,\mathbf{T}_E^F(m,m)]\boldsymbol{\Phi}_B(z',m) - \Delta z'\,\mathbf{T}_E^B(m,m)\boldsymbol{\Phi}_F(z',m) - \Delta z' \sum_{n\le m} \mathbf{T}_I(m,n)\boldsymbol{\Phi}_B(z',n), \quad (22b)$$

where z' and $\Delta z'$ are $z/\cos\theta_m$ and $\Delta z/\cos\theta_m$, respectively.

$\boldsymbol{\Phi}(z)$ is now rewritten as

$$\boldsymbol{\Phi}(z) = [\boldsymbol{\Phi}^F(z),\boldsymbol{\Phi}^B(z)] = [\boldsymbol{\Phi}^F(z,1), \boldsymbol{\Phi}^F(z,2), \ldots, \boldsymbol{\Phi}^F(z,m), \ldots, \boldsymbol{\Phi}^B(z,1), \times \boldsymbol{\Phi}^B(z,2), \ldots, \boldsymbol{\Phi}^B(z,m), \ldots],$$

where the energy level of the incident electrons is denoted by $m = 1$. Equations (22a) and (22b) can be reduced to the same formula as (17). In this case, the transition matrix has the following form:

$$\mathbf{T} = \begin{pmatrix} \mathbf{T}_A & \mathbf{T}_B \\ -\mathbf{T}_B & -\mathbf{T}_A \end{pmatrix}, \quad (23)$$

where

$$\mathbf{T}_A = \begin{pmatrix} \mathbf{T}_E^F(1,1) & & 0 & \\ \mathbf{T}_I(2,1) & \mathbf{T}_E^F(2,2) & & \\ \mathbf{T}_I(3,1) & \mathbf{T}_I(3,2) & \mathbf{T}_E^F(3,3) & \\ . & . & . & . \end{pmatrix}, \quad (24a)$$

and

$$\mathbf{T}_B = \begin{pmatrix} \mathbf{T}_E^B(1,1) & & 0 & \\ & \mathbf{T}_E^B(2,2) & & \\ & & \mathbf{T}_E^B(3,3) & \\ 0 & & & . \end{pmatrix}. \quad (24b)$$

From symmetry in (23), the orthogonal matrix $\mathbf{C}$ leads to

$$\mathbf{C} = \begin{pmatrix} \mathbf{C}_1 & \mathbf{C}_2 \\ \mathbf{C}_2 & \mathbf{C}_1 \end{pmatrix}, \quad (25)$$

and the eigenmatrix $\boldsymbol{\Lambda}$ becomes

$$\boldsymbol{\Lambda} = \begin{pmatrix} \boldsymbol{\Lambda}_a & \mathbf{0} \\ \mathbf{0} & \boldsymbol{\Lambda}_a \end{pmatrix}, \quad (26)$$

where

$$\boldsymbol{\Lambda}_a = \begin{pmatrix} -\lambda_1, & & 0 & \\ & -\lambda_2, & & \\ & & -\lambda_3, & \\ 0 & & & . \end{pmatrix}, \quad (\lambda_i > 0 \text{ for all } i\text{'s}). \quad (27)$$

To obtain intensities of back-scattered electrons, the following boundary conditions are applied:

$$\boldsymbol{\Phi}^F(0,j,1) = C_0^i(\mathbf{k}_0)\delta_{\mathbf{k}j,\mathbf{k}_0 i}, \quad (28a)$$

$$\boldsymbol{\Phi}^B(D,j,m) = \mathbf{0}, \quad \text{for all } m\text{'s and } j\text{'s}. \quad (28b)$$

These relations have been used in the theory of electron-channelling patterns (Hirsch & Humphreys, 1970; Spencer & Humphreys, 1973). In the case of semi-infinite specimens ($D \to \infty$), using (20), (25), (26) and (28), we can obtain

$$\boldsymbol{\Phi}^B(z) = \mathbf{C}_2\,\mathbf{C}_1^{-1}\,\boldsymbol{\Phi}^F(z) \quad (29)$$

and

$$\boldsymbol{\Phi}^F(z) = \mathbf{C}_1 \exp(\boldsymbol{\Lambda}_a)\,\mathbf{C}_1^{-1}\,\boldsymbol{\Phi}^F(0). \quad (30)$$

The derivation of (29) and (30) is due to Fathers & Rez (1978) from their theory of back-scattering yield for noncrystalline specimens.

3. Procedures for calculations

Elements of the transition matrix were evaluated in the case of thin specimens by applying the two-beam approximation to (16). As interaction potentials, the excitation of phonons and core electrons was taken into account, while plasmon excitation was excluded since it causes inelastic scattering at extremely small angles. Then, $S_{gh}(\mathbf{q}_0)$ in (16) was given by the sum of $S_{gh}^{\rm ph}$ and $S_{gh}^{\rm cr}$. For the excitation of phonons (Hall & Hirsch, 1965),

$$S_{gh}^{\rm ph}(\mathbf{q}_0) = f(q_g)f(q_h)\{\exp[-\alpha'(g-h)^2] - \exp[-\alpha'(q_g^2+q_h^2)]\}/\Omega, \quad (31)$$

where Ω is the atomic volume, α' is the constant for the Debye–Waller factor and $f(q)$ is the atomic scattering amplitude. For the excitation of core electrons, we used an approximate expression given in the previous study (Yamamoto, Mori & Ishida, 1978),

$$S_{gh}^{\rm cr}(q_0) = (me^2/2\pi^2\hbar^2)^2[Zq_s^2/\Omega(q_g^2+q_t^2)(q_h^2+q_t^2)] \times \{1/[(g-h)^2+q_s^2] - q_s^2/(q_g^2+q_s^2)(q_h^2+q_s^2)\}, \quad (32)$$

where Z is the atomic number, q_s^2 is the screening factor [$q_s^2 = me^2/2\pi^2\hbar^2 f(0)$], $q_t = k\Delta E/E$ (k is the wavenumber of the incident electrons, ΔE is the mean ionization energy, $11{\cdot}5Z$ eV and E is the energy of the electrons). This expression approximately coincides with that derived by Lenz (1954) when q_0 approaches zero, and for $g \neq h = 0$, as shown by Yoshioka (1957), $S_{gh}^{\rm cr}(\mathbf{q}_0)$ is always positive when $\mathbf{q}_0$ is perpendicular to $\mathbf{g}$ and negative when $q_0 < g$ ($\mathbf{q}_0$ is parallel to $\mathbf{g}$). In addition, the value of the expression in the curly brackets in (32) is of the same order of magnitude as

that derived from a more exact calculation (Humphreys & Whelan, 1969).

The number of matrix elements in this calculation was reduced by the following procedure: each dispersion surface was divided into several rectangular areas except for the following two areas; the ring-shaped area with radii of $w = 20$ and 100 (w is the deviation parameter used in the two-beam approximation), and the infinitely small (point-like) area which corresponded to the incident direction. Inelastic scattering processes transferred beyond the ring-shaped area were neglected. One of the margins of the above rectangular areas was chosen to be parallel to the x axis on the dispersion surface, the axis being parallel to the reciprocal vector $\mathbf{g}$ of the operating reflection. Then, the excitation weights were assumed to be the same over each divided area. Since, moreover, the excitation weights were symmetric with respect to the x axis, we restricted ourselves only to the area whose center lay on $x \geq 0$. By so doing, each dispersion surface was divided into 37 areas in the present calculation.

The value of the matrix elements was determined by integrating (16) over each divided area. The integration was normally carried out by using 8-point values of S_{gh}. $S^{cr}_{hh}(\mathbf{q}_0)$ ($h = 0$, g or $\bar{g}$) occasionally showed a steep rise at positions $q_h \simeq 0$. In such cases, 16-point values were used. After these procedures, $T_{\mathbf{k}'j,\mathbf{k}i}$ inside the outer-ring area were slightly corrected so as to satisfy the self-consistent relation of (18): this was performed by multiplying the initially calculated value of $T_{\mathbf{k}'j,\mathbf{k}i}$ by $-\mu_i(\mathbf{k}_i)/\sum'_{\mathbf{k}'j}\, \mathbf{k}i$.

Excitation weights were calculated for Cu 200 and Si 220 reflections at an accelerating voltage of 100 kV, setting the incident beam at the Bragg position ($w = 0$) or slightly outside the position ($w = 3{\cdot}5$). Finally, excitation weights were determined by interpolating the histogram of $\Phi(z)$ obtained with the above calculations.

4. Results and discussion

4.1. *Calculated excitation weights*

Figs. 2(a) and 3(a) show excitation weights calculated at $w = 0$ for Cu and Si, which are plotted against k_x. In this case, excitation weights at $k_x < 0$ are omitted due to symmetry with respect to the y axis. A large peak at $k_x = 0$ results from the excitation of core electrons. Matrix elements at such divided areas ($k_x \simeq 0$) can approximately be expressed as*

$$T_{\mathbf{k}'j,\mathbf{k}i} = 2\alpha' g^2 f(g)^2 (C^i_0 C^j_g - C^i_g C^j_0) + S^{cr}_{00}(0)(C^i_0 C^j_0 + C^i_g C^j_g).$$

* The first term in this equation is approximately derived from (31) by using the single-phonon excitation only. This term coincides with that derived from $H^s_g(\mathbf{q}_0)$ given by Takagi (1958a) when the element is determined from the longitudinal phonon scattering in the Einstein Model (Whelan, 1965b).

From this equation, it is seen that the phonon excitation causes the inter-band transition (Takagi, 1958a), whereas the excitation of core electrons causes the intra-band transition (Howie, 1963). The latter excitation is predominantly responsible for the large peak. A similar peak appears at $k_x = G$, which results from the diffraction effect on the waves proceeding in the $\mathbf{k}_0$ direction. The matrix element of the transfer to this area on the dispersion surface can approximately be given by

$$T_{\mathbf{k}'j,\mathbf{k}i} = S^{cr}_{gg}(g) C^{i2}_g + 2S^{cr}_{g0} C^j_0 C^j_g C^{i2}_g + 2C^i_0 C^i_g S^{cr}_{gg}(g) C^j_0 C^j_0 + 2\alpha' g^2 f(g)^2 [(C^i_0 C^j_0 + C^i_g C^j_g)^2 + 4C^{i2}_0 C^{j2}_g].$$

This equation indicates a strong transition towards the branch 2 which results from the excitation of core electrons.

Figs. 2(b) and 3(b) show excitation weights plotted against k_x under the same conditions as in the above. It appears that large-angle scattering along the k_y direction gives rise to a greater probability of electrons falling on branch 2. It is found that at very small thicknesses (200 Å for Cu and 500 Å for Si) $|\psi^2(D)|^2$ is greater than $|\psi^1(D)|^2$. However, as the thickness increases $|\psi^1(D)|^2$ becomes larger, as shown in Figs. 2

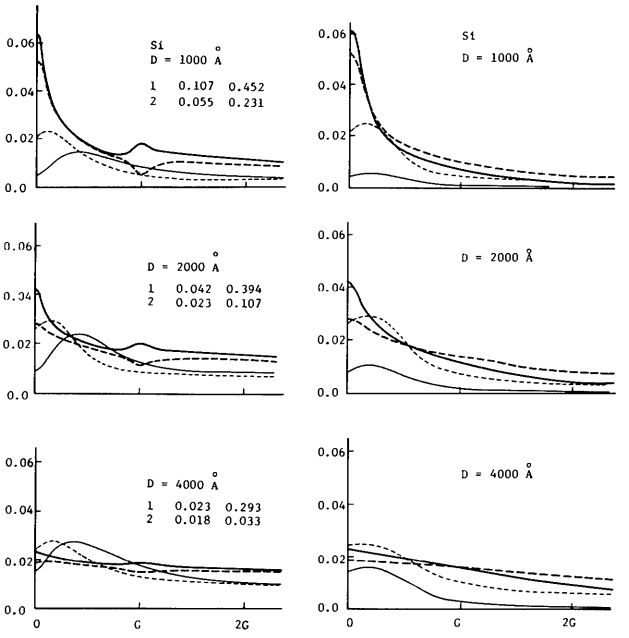

Fig. 2. Excitation weights on dispersion surfaces for the Si 220 reflection at an incidence of $w = 0$: (a) in the k_x direction; (b) in the k_y direction. Solid and dashed lines indicate the weights in branches 1 and 2, respectively. Thin lines are obtained with the phonon scattering only. Tables in (a) show the weights at the point area ($\mathbf{k} = 0$): upper and lower numerical values are the weights for branches 1 and 2, respectively, and left and right values are obtained with and without the excitation of core electrons.

and 3. This is due to the effect of anomalous absorption on Bloch waves of branch 2, *i.e.* to the reduced excitation weights of the waves. Such a reduction is more prominent for Bloch waves preserving the initial incidence state ($\mathbf{k} = \mathbf{0}$), as given in the tables of Figs. 2(*a*) and 3(*a*). Neglecting a minor contribution of S_{gh}^{cr}, the scattering probability for $q_0 \geq g$ is given by

$$\sum_{\mathbf{k},i} T_{\mathbf{k}'j,\mathbf{k}i} = [\alpha' q_0^2 f(q_0)^2 + \alpha'(q_0^2 + g^2) f(q_g)^2] + (-1)^i 2\alpha' g^2 f(q_0) f(q_g).$$

It is clear that as the scattering angle increases the transition to branch 2 becomes predominant due to phonon excitation. This fact has already been shown by Kamiya & Nakai (1971). Moreover, Kamiya & Shimizu (1976) studied the contrast reversal of Kikuchi bands by evaluating the difference between $|\psi^1(D)|^2$ and $|\psi^2(D)|^2$. In their case, a Monte Carlo simulation was used, substantially based on the transport equation. These authors' results of $|\psi^i(D)|^2$ along k_y for the Ag 220 reflection show trends similar to those in the present calculation.

In any case, when compared with the excitation weights evaluated by the phonon scattering only, the increase in the weights over almost all the areas in the dispersion surfaces stems from high-angle scattering of electrons which are initially scattered at small angles due to the excitation of core electrons. In view of this fact, values of excitation weights in relatively thick specimens are sensitively affected by the detailed profile of $S_{gh}^{cr}(\mathbf{q}_0)$, especially at $q_0 < g$. In the present calculation, the Lenz (1954) approximation was used for (32) by including the energy dispersion relation of the effective wave-vector transfer q, *i.e.* $q^2 = q_0^2 + q_t^2$. On account of the sensitivity of S_{gh}^{cr} as shown above, a more accurate determination of S_{gh}^{cr} is desired, for example, using Freeman's (1959) data.

In Fig. 4, a similar peak of the excitation weights appears in the vicinity of $k_x = 0$, where the incident condition is $w = 3{\cdot}5$. This is also due to the diffraction effect *via* the excitation of core electrons. Bloch waves belonging to branches 1 and 2 for reflection $\bar{G}$ also show a marked anomalous transmission or absorption at $k_x = -g$. It can be anticipated therefore that the waves scattered in such areas mainly by the excitation of core electrons as seen in Fig. 4 changes the values of $\Phi(D)$ calculated in the two-beam approximation. The actual profile of $\Phi(D)$ at the incidence of $w = 0$ is by no means symmetric with respect to the y axis, but rather

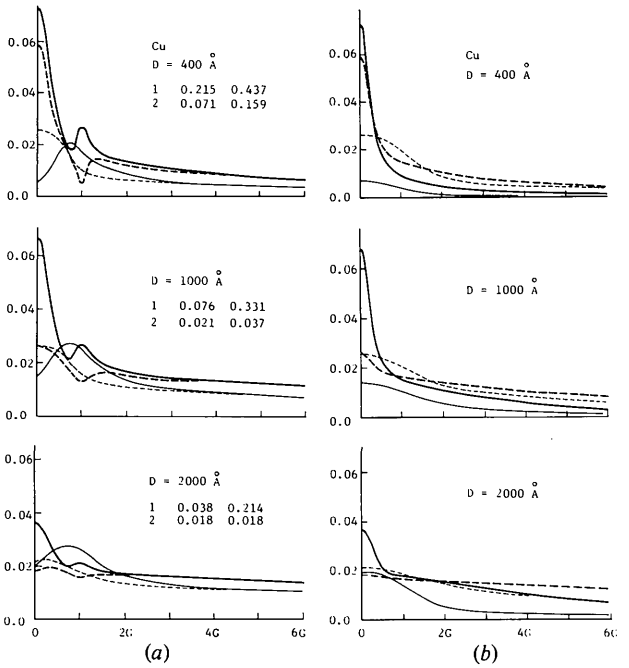

Fig. 3. Excitation weights on dispersion surfaces for the Cu 200 reflection at an incidence of $w = 0$: (*a*) in the k_x direction; (*b*) in the k_y direction. The meaning of the lines and the numerical values in the tables are the same as in Fig. 2.

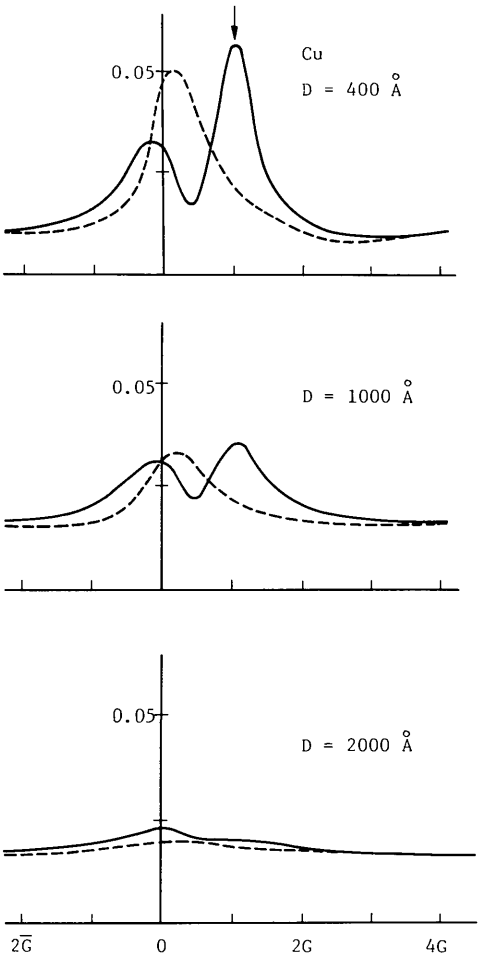

Fig. 4. Excitation weights on dispersion surfaces for the Cu 200 reflection at an incidence of $w = 3{\cdot}5$. The meaning of lines is the same as in Fig. 2. The arrow indicates the incident direction.

symmetric to the plane of $k_x = g/2$ when the specimen thickness increases. It is desired to evaluate $\Phi(D)$ in the three-beam approximation at least. This problem may be solved using a computer with large storage.

4.2. *Cross terms of Bloch-wave amplitudes and some remarks*

The cross terms, $\psi^j_{\mathbf{k}'}(z)\ \psi^{i*}_{\mathbf{k}}(z)$, neglected in (4) are related to the interference fringes in the intensities of diffusely scattered electrons because of the difference in wave vector. Neglecting the terms implies that only the background of the intensities is treated in the present theory. Resonance error δk^{ji}_{mnz} is in proportion to the inverse of the specimen thickness, *i.e.* $\delta k^{ji}_{mnz} = l/D$ (l, integer). When, therefore, the exponential coefficients in (4) are evaluated by averaging them over all possible values of $\delta \mathbf{k}^{ji}_{mn}$, the coefficients contain the factor

$$\overline{\sum \exp(-2\pi\delta k^{ji}_{mnz} z)} = \exp[-a(z/D)^2],$$

where $a = 4\pi^2 \sum \bar{l}^2$. This factor suggests that the cross terms provide a rather weaker contribution to the final value of $\psi^j_{\mathbf{k}'}(D)\ \psi^{i*}_{\mathbf{k}}(D)$ in the vicinity of the bottom of the specimen.

Equation (22) is identical, in its form, with that derived for noncrystalline specimens based on a transport equation (Spencer, 1955; Dashen, 1964; Fathers & Rez, 1978). In the latter theory, the quantities evaluated are electron fluxes while they are excitation weights of Bloch waves in the present theory. An excitation weight is not directly related to an electron flux, but to the intensity of a Bloch wave proceeding in various diffracted-beam directions. It can easily be verified that when the beam direction is greatly deviated from the Bragg position, $|\psi^i_{\mathbf{k}}(z)|^2$ tends to the flux in the $\mathbf{k}$ direction. Besides, if desired, (8) can be transformed to that for the electron fluxes using a linear transformation within the framework of the approximation in which the interference terms can be neglected.

Rez (1978) has discussed an identity between the transport equation and the solution of Howie's equations in a more general form which includes the cross terms. It appears in the present theory that the complete identity can be achieved when all the cross terms are neglected. It should be noted, moreover, that in practical calculations including the cross terms induces a serious difficulty in the storage of the computer; when the number of the divided areas in the dispersion surfaces is N, the number of excitation weights is N, whereas that of the cross terms is $N(N-1)$. Eventually, the number of transition matrix elements becomes N^2 and N^4 for the former and latter cases, respectively.

The storage problem becomes more serious in the case of high-angle scattered electrons. Equation (23) contains many zero off-diagonal submatrices. In addition, all non-zero submatrices can be characterized by only three submatrices, $\mathbf{T}_I$, $\mathbf{T}^F_E$ and $\mathbf{T}^B_E$, at a certain energy (*e.g.* those at the energy of the incident electrons) and by several proportional coefficients which are determined from the dependence of the elements on the electron energy. Taking into account these facts, Fathers & Rez (1978) developed a method for diagonalizing (23) with a reduced storage. In fact, these authors succeeded in calculating the yield of back-scattered electrons in noncrystalline specimens; in particular, good agreement with experiment was found regarding the dependence of the yield on the atomic number, the emitting angle and the energy of back-scattered electrons. Their method may encourage others to attack multiple inelastic scattering processes in crystalline specimens.

In crystalline specimens, however, there are some precautions made in practical calculations: (1) the division of dispersion surfaces must be made finer compared with that in noncrystalline specimens, because a rapid change in Bloch-wave coefficients $C^i_g(\mathbf{k})$ appears in the vicinity of Bragg positions, and (2) as shown in § 4.1, the values of excitation weights are markedly affected by the detailed profile of S^{cr}_{gh} resulting from the excitation of core electrons. At present, the profile may still be uncertain in a greater or lesser degree.

The author thanks Dr Y. Ishida (University of Tokyo) for providing the computer facility used in this calculation. He also wishes to extend his thanks to Dr Peter Rez (University of California) and Dr David J. Fathers (University of Oxford) for showing him their preprint and personal communications.

References

DASHEN, R. F. (1964). *Phys. Rev. Sect. A*, **134**, 1025–1032.
FATHERS, D. J. & REZ, P. (1978). Proc. 13th Annu. Conf. on Microbeam Analysis, Michigan, pp. 40–46.
FREEMAN, A. J. (1959). *Acta Cryst.* **12**, 274–283.
FUJIMOTO, F. & KAINUMA, Y. (1963). *J. Phys. Soc. Jpn*, **18**, 1692–1701.
HALL, C. R. & HIRSCH, P. B. (1965). *Proc. R. Soc. London Ser. A*, **286**, 158–177.
HIRSCH, P. B. & HUMPHREYS, C. J. (1970). Proc. 3rd Annu. SEM Symposium, pp. 449–454. Chicago: IIT Research Institute.
HOWIE, A. (1963). *Proc. R. Soc. London Ser. A*, **271**, 268–287.
HUMPHREYS, C. J. & WHELAN, M. J. (1969). *Philos. Mag.* **20**, 165–172.
KAINUMA, Y. (1955). *Acta Cryst.* **8**, 247–257.
KAMIYA, Y. & NAKAI, Y. (1971). *J. Phys. Soc. Jpn*, **31**, 195–203.
KAMIYA, Y. & SHIMIZU, R. (1976). *Jpn J. Appl. Phys.* **15**, 2067–2072.
LENZ, F. (1954). *Z. Naturforsch Teil A*, **9**, 185–204.
OKAMOTO, K., ICHINOKAWA, T. & OHTSUKI, Y. (1971). *J. Phys. Soc. Jpn*, **30**, 1690–1701.

REZ, P. (1978). *Electron Diffraction*, 1927–1977, pp. 61–67. London: Institute of Physics.
SPENCER, J. P. & HUMPHREYS, C. J. (1973). *Scanning Electron Microscopy: Systems and Applications*, pp. 126–131. London: Institute of Physics.
SPENCER, L. V. (1955). *Phys. Rev.* **98**, 1597–1615.
TAKAGI, S. (1958*a*). *J. Phys. Soc. Jpn*, **13**, 278–286.
TAKAGI, S. (1958*b*). *J. Phys. Soc. Jpn*, **13**, 287–296.
WHELAN, M. J. (1965*a*). *J. Appl. Phys.* **36**, 2099–2103.
WHELAN, M. J. (1965*b*). *J. Appl. Phys.* **36**, 2103–2110.
YAMAMOTO, T., MORI, M. & ISHIDA, Y. (1978). *Philos. Mag.* **38**, 439–461.
YOSHIOKA, H. (1957). *J. Phys. Soc. Jpn*, **12**, 618–628.

Acta Cryst. (1980). A**36**, 134–139

X-ray Diffraction from Nonstoichiometric Titanium Sulfide Containing Stacking Faults

BY M. ONODA AND I. KAWADA

National Institute for Researches in Inorganic Materials, Sakura-mura, Niihari-gun, Ibaraki, 300-31, *Japan*

(*Received* 16 *June* 1979; *accepted* 22 *August* 1979)

Abstract

The layer units appropriate to the analysis of titanium sulfide with stacking faults are considered. The layer units composed of one sulfur layer and one titanium layer are adopted for the structures whose stacking sequences are relatively simple. The layer units composed of two sulfur layers, one fully occupied titanium layer, half of a partly occupied titanium layer and half of another partly occupied titanium layer are adopted in the case of the more complex stacking sequences. The general method for obtaining the diffraction intensity distribution by matrices is modified so as to be suitable for the analysis based on these layer units, and examples of the calculated intensity curves are illustrated.

Introduction

It is often observed that selective broadening and weakening occurs for reflexions with $h - k \neq 3n$ (hkl; indices on the hexagonal cell of the close-packing layers of sulfur) in the X-ray diffraction pattern of nonstoichiometric titanium sulfide. This broadening and weakening suggests the occurrence of stacking faults. For the analysis of structures with stacking faults, the theoretical intensity distribution formulas were derived by Wilson (1942), Hendricks & Teller (1942), Jagodzinski (1949*a*,*b*), Paterson (1952), Kakinoki & Komura (1952, 1954*a*,*b*, 1965) and Kakinoki (1965, 1966, 1967). The scattering powers are not the same for all the layers in the case of nonstoichiometric titanium sulfide, so the derivation of the expression available for this system is required.

In this paper we consider the layer units appropriate to the titanium–sulfur system and propose a modified procedure to calculate the intensity distribution by using the matrix method given by Kakinoki & Komura.

The structures of titanium sulfides

In the range TiS–TiS_2, several phases such as TiS, Ti_8S_9, Ti_4S_5, Ti_3S_4, Ti_2S_3, Ti_5S_8 and TiS_2 have been found (Jeannin, 1962; Wiegers & Jellinek, 1970; Tronc & Huber, 1973). The structures of these phases are all based on close-packing layers of sulfur; hexagonal close packing for TiS or TiS_2, and more complex stacking sequences of *h*-packed sulfur layers and *c*-packed sulfur layers for the intermediate phases. Titanium atoms always occupy octahedral holes in the close-packing structure of sulfur. These sites are fully and partly occupied in the alternating titanium layers in the composition range $TiS_{1.4}$ to TiS_2, which corresponds to the existence range of the phases Ti_2S_3, Ti_5S_8 and TiS_2. We will discuss such a range, then three kinds of layers are considered; that is sulfur layers, fully occupied titanium layers and partly occupied titanium layers. They are represented by S, Ti and Ti′, respectively. The common feature of stacking is represented by ...STiSTi′STiSTi′S... as shown in Fig. 1. We assume that this common feature of stacking is maintained throughout the faulted structure

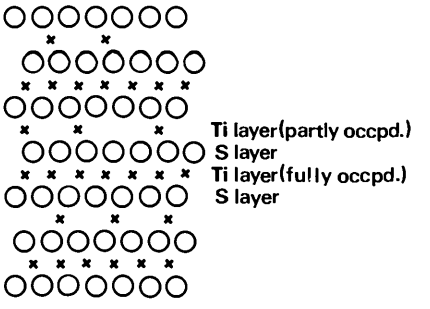

Fig. 1. Schematic drawing of the common stacking features in the range $TiS_{1.4}$ to TiS_2.

0567-7394/80/010134-06$01.00 © 1980 International Union of Crystallography